



This is a repository copy of *The Theory of Critical Distances to assess failure strength of notched plain concrete under static and dynamic loading*.

White Rose Research Online URL for this paper:

<https://eprints.whiterose.ac.uk/118968/>

Version: Accepted Version

Article:

Pelekis, I. and Susmel, L. orcid.org/0000-0001-7753-9176 (2017) The Theory of Critical Distances to assess failure strength of notched plain concrete under static and dynamic loading. *Engineering Failure Analysis*, 82. pp. 378-389. ISSN 1350-6307

<https://doi.org/10.1016/j.engfailanal.2017.07.018>

Reuse

This article is distributed under the terms of the Creative Commons Attribution-NonCommercial-NoDerivs (CC BY-NC-ND) licence. This licence only allows you to download this work and share it with others as long as you credit the authors, but you can't change the article in any way or use it commercially. More information and the full terms of the licence here: <https://creativecommons.org/licenses/>

Takedown

If you consider content in White Rose Research Online to be in breach of UK law, please notify us by emailing eprints@whiterose.ac.uk including the URL of the record and the reason for the withdrawal request.



eprints@whiterose.ac.uk
<https://eprints.whiterose.ac.uk/>

The Theory of Critical Distances to assess failure strength of notched plain concrete under static and dynamic loading

Iason Pelekis^a, Luca Susmel^b

^aDepartment of Engineering, University of Cambridge,
Trumpington Street, Cambridge, CB2 1PZ, United Kingdom

^bDepartment of Civil and Structural Engineering, The University of Sheffield,
Mappin Street, Sheffield, S1 3JD, United Kingdom

ABSTRACT

The Theory of Critical Distances (TCD) is a design method that is widely used in situation of practical interest to estimate the strength of notched/cracked components subjected to either static, dynamic, or fatigue loading. The TCD makes use of a characteristic length to post-process the linear-elastic stress fields damaging the material in the vicinity of the stress concentrators being designed. The employed length scale parameter depends on the specific microstructural features of the material under investigation. By making the most of the TCD's unique features, the present paper summarises an attempt of reformulating this powerful theory to make it suitable for assessing static and dynamic strength of notched plain concrete. The accuracy and reliability of the proposed reformulation of the TCD is checked against a number of experimental results that were generated by testing, under different displacement rates, square section beams of plain concrete containing notches of different sharpness. This validation exercise allowed us to demonstrate that the proposed reformulation of the TCD, which is based on the use of simple power laws, is capable of accurately assessing the static and dynamic strength of the notched un-reinforced concrete being tested, with the estimates falling within an error interval of $\pm 20\%$. The obtained level of accuracy is certainly satisfactory, especially owing to the fact that static and dynamic strength is predicted without explicitly modelling those non-linearities characterising the stress vs. strain dynamic behaviour of concrete.

Keywords: Un-reinforced concrete, notch, static loading, dynamic loading, critical distance.

NOMENCLATURE

a_f, b_f	material constants in the σ_f vs. $\dot{\epsilon}$ relationship
a_K, b_K	material constants in the K_{Id} vs. $\dot{\epsilon}$ relationship
$f_{\sigma_0}(\dot{Z})$	calibration function for $\sigma_0(\dot{Z})$.
$f_{\sigma_f}(\dot{Z})$	calibration function for $\sigma_f(\dot{Z})$
$f_{K_{Id}}(\dot{Z})$	calibration function for $K_{Id}(\dot{Z})$
r_n	notch root radius
x	generic material property
x_d	value of material property x under dynamic loading
x_s	value of material property x under quasi-static loading
DIF	Dynamic Increase Factor
K_{Ic}	plane strain fracture toughness
K_{Id}	dynamic fracture toughness
K_t	stress concentration factor
L	critical distance
Oxyz	system of coordinates
\dot{Z}	reference dynamic variable
α_L, β_L	material constants in the L vs. \dot{Z} relationship
$\alpha_{\sigma_0}, \beta_{\sigma_0}$	material constants in the σ_0 vs. \dot{Z} relationship
$\dot{\epsilon}$	strain rate
$\dot{\epsilon}_s, \gamma_s, \alpha_s$	reference constants in Table 1
σ_0	inherent strength
σ_1	maximum principal stress
σ_{cs}	static uniaxial compressive strength
σ_{eff}	effective stress
σ_f	failure stress
σ_{fn}	notch failure nominal stress referred to the net area
σ_{nom}	nominal stress
σ_y	normal stress parallel to axis y
σ_{UTS}	ultimate tensile strength
θ, r	polar coordinates
$\dot{\Delta}$	displacement rate

1. Introduction

In situations of practical interest (such as under either blast or impact loading), concrete structures have to be designed to withstand high stress/strain rates. Having recognized this as a complex structural engineering problem, since about the middle of the last century, the international scientific community has made a tremendous effort to understand and model the mechanical/cracking behaviour of concrete materials subjected to dynamic loading. This issue has been addressed extensively by tackling this problem both from an experimental and a theoretical angle. Following the pioneering work done by Hopkinson, Davies and Kolsky [1–3] as well as Mellinger and Birkimer [4] used high velocity projectiles to strike concrete cylindrical specimens and induce spalling failure under high strain rate conditions. Since then, a number of experimental investigations (see, for instance, Refs. [5, 6] and the references reported therein) have confirmed that, at room temperature, both the compressive and tensile strength of concrete tend to increase with the increase of the loading/displacement/strain rate.

After the advent of Linear Elastic Fracture Mechanics (LEFM), a few investigations were carried out also to study the existing relationship between material fracture toughness and loading rate. In particular, much experimental evidence [7, 8] suggests that, at room temperature, concrete's fracture toughness can either remain constant or increase as the Stress Intensity Factor (SIF) rate increases, this mainly depending on the existing interactions between crack propagation mechanisms and material micro/meso-structural features.

Despite the large body of knowledge available to structural engineers designing concrete structures against dynamic loading, examination of the state of the art shows that a commonly accepted design approach has not yet been agreed by the international scientific community. Furthermore, the sensitivity of concrete to the presence of finite radius notches has never been investigated systematically in the past. Consequently, there are no specific approaches suitable for designing notched plain concrete against static and dynamic loading.

In this challenging scenario, by taking full advantage of the so-called Theory of Critical Distances, the present paper reports on an attempt of formulating a unifying design methodology suitable for performing static/dynamic assessment of notched plain concrete.

2. Mechanical/Cracking behaviour of plain concrete under dynamic loading

Concrete is a three phase material (i.e., cement paste, aggregates, and transition zone) whose mechanical properties vary locally. When concrete is loaded dynamically, cracks are seen to propagate through those material regions characterised by higher local resistance, causing aggregate interlocking or further micro-cracking [9–11]. On the contrary, under very low loading rates, the stiffness and toughness of the aggregates can lead to crack deflection, forcing the cracks themselves to grow along those paths requiring the least amount of energy for the propagation process to take place [9–12]. Furthermore, under low loading rates, large voids can arrest the crack growth process [13], with this resulting in an apparent increase of the material's resistance to the propagation of cracks.

Examination of the state of art shows that the effect of the loading rate on the overall mechanical/cracking behaviour of concrete is usually quantified in terms of Dynamic Increase Factor (DIF). In particular, for a given material property, the DIF is the ratio between the value of the specific material property being investigated under dynamic, x_d , and quasi-static, x_s , loading, respectively, i.e. [14-16]:

$$DIF = \frac{x_d}{x_s} \quad (1)$$

The testing of un-notched un-confined concrete specimens under high loading rates is the typical procedure that is followed to quantify the DIF in terms of strength. The most common experimental methodologies involve the use of split Hopkinson pressure bars (SPHBs) and the combined use of SHPBs and Brazilian splitting specimens to investigate the mechanical behaviour

of concrete under compression and tension, respectively. It is worth observing here that, apart from conventional cracking, these experimental techniques are seen to activate additional mechanisms that affect the overall strength of concrete. In particular, much experimental evidence suggests that, under strain rates larger than about 200 s^{-1} , the lateral inertia of the cylindrical specimens placed between the two loading bars of the SHPBs confines the material, with this resulting in an increase of its strength [6, 17]. In contrast, the triaxial tensile stresses that result from uniaxial dynamic loading waves prevent the additional strengthening mechanisms associated with the inertia from activating themselves, with this leading to DIF values that are conservative [18]. In addition, since under dynamic loading the free water in the concrete's pores remains viscous, Stefan's effect has been identified as another possible mechanism that can further increase the compressive and tensile strength of concrete under high loading/strain rates [12, 19, 20].

By focusing their attention on the failure stress of un-reinforced concrete subjected to tensile loading, Malvar and Crawford [21] have observed that the increase of the DIF (defined as the ratio between the tensile strength under a specific strain rate and the corresponding strength under quasi-static loading) with the increase of the strain rate can be subdivided into two different regimes. In more detail, according to Figure 1, the increment in strength is seen to be quite limited up to a strain rate, $\dot{\epsilon}$, of 1 s^{-1} . In this regime, final breakage is mainly governed by the same mechanisms as those commonly observed under quasi-static loading. As soon as the applied strain rate, $\dot{\epsilon}$, becomes larger than about 1 s^{-1} , the material cracking behaviour becomes more complex, with the associated failure mechanisms leading to a very rapid growth of the tensile DIF as the applied strain rate increases (Fig. 1).

Having recognised that the employed experimental techniques can create an apparent increase in the tensile/compressive DIF and that various mechanisms counteracting each other may manifest themselves, modelling the dynamic behaviour of concrete structures is never a simple task. Table 1 summarises the most popular approaches that, since about the middle of the last century, have

been devised (and somehow validated) to estimate dynamic strength of concrete [22, 23]. The governing equations reported in Table 1 are in the form of logarithmic polynomials that fit the experimental data, with strain rate $\dot{\epsilon}$ being the independent variable. These different models have been derived based on the interpolation of datasets generated by testing materials having specific mechanical properties [23]. Therefore, there is little flexibility to adjust these models to make them suitable for modelling the mechanical/strength behaviour of concrete mixes with different material properties (e.g. strength). An interesting exception is represented by the CEB model [25]. In particular, since the calibration of this model for the estimation of the tensile strength involves a number of parameters that can be adjusted, its applicability is obviously wider.

By carefully observing the different models that are summarised in Table 1, it is interesting to point out that, after some manipulations, all these equations, even if they are sometimes very complex, can all be brought back to the following simple form:

$$\sigma_f(\dot{\epsilon}) = a_f \cdot \dot{\epsilon}^{b_f} \quad (2)$$

In other words, examination of the state of the art suggests that all the models that have been proposed so far to link the dynamic strength, σ_f , of un-reinforced concrete to the rate of the applied strain, $\dot{\epsilon}$, can be rewritten in the form of power laws, where, according to Eq. (2), a_f and b_f are material constants that have to be estimated by running appropriate experiments.

Even though much work has been done to determine the variation of the strength DIF with respect to the strain rate, solely a limited number of studies investigating the variation of the fracture toughness of un-reinforced concrete as the rate of the applied loading increases are available in the technical literature. Midness et al. [33] tested notched concrete beams under impact loading by realising a hammer from specific heights. According to the generated experimental results, they came to the conclusion that concrete becomes tougher and tougher as the hammer's drop height increases, but no explicit relationship between loading rate and fracture toughness was

proposed. An attempt of modelling the fracture behaviour of plain concrete under dynamic loading was made instead by Reji & Shah in 1990 [7]. In more detail, they used a two-parameter fracture model based on the crack opening displacement and the fracture toughness to reanalyse their results. According to Reji & Shah's experimental/theoretical outcomes, it is possible to conclude that, in the low loading rate regime, the fracture toughness of plain concrete should increase moderately as the loading rate itself increases.

In 2000 Lambert & Ross [8] performed a systematic experimental investigation by using a SHPB to test Brazilian splitting tensile specimens containing internal notches, with this experimental configuration allowing them to achieve higher strain rates than those investigated by Reji & Shah [7]. The data being generated were then post-processed by employing a modified two parameter fracture model. According to this experimental/theoretical investigation, Lambert & Ross as well came to the conclusion that the fracture toughness of plain concrete increases as the strain rate increases [8].

If the experimental results generated by Reji and Shah [7] as well as by Lambert and Ross [8] are reported in a log-log diagram plotting the fracture toughness, K_{Id} , vs. the applied strain rate, $\dot{\epsilon}$ (see Figure 2), it is straightforward to observe that, similar to the σ_f vs $\dot{\epsilon}$ behaviour shown in Figure 1, the dynamic fracture toughness increases as the strain rate increases according to a simple power law, i.e.:

$$K_{Id}(\dot{\epsilon}) = a_K \cdot \dot{\epsilon}^{b_K} \quad (3)$$

with a_K and b_K being material constants to be determined experimentally. As to Figure 2, it is worth observing that, for the different experimental results being reported, the fracture toughness was defined via the effective value of the stress intensity factor, i.e. by referring the SIF value to the crack length at failure.

To conclude, it can be pointed out that Eqs (2) and (3) represent the fundamental mathematical tools on which the novel formalisation of the TCD proposed in the present paper will be based, with the formulation and validation of this new failure assessment methodology being discussed in Sections 4 and 6, respectively.

3. Fundamentals of the Theory of Critical Distances under quasi-static loading

The TCD postulates that notched components subjected to Mode I quasi-static loading do not fail as long as the following condition is assured [34, 35]:

$$\sigma_{\text{eff}} < \sigma_0 \quad (4)$$

In inequality (4) σ_{eff} is the effective stress determined according to the TCD, whilst σ_0 is the so-called inherent material strength. If the TCD is used to perform the static assessment of brittle notched materials, σ_0 can be taken equal to the material ultimate tensile strength, σ_{UTS} [36]. In contrast, as far as ductile notched materials are concerned, σ_0 is seen to be larger than σ_{UTS} [37-39], with the determination of σ_0 requiring complex, time-consuming and expensive experiments [34, 37].

Critical distance L is the second material property which is needed to apply the TCD to design notched components in situations of practical interest. Under quasi-static loading, this length scale parameter can be estimated directly from the plane strain fracture toughness, K_{Ic} , and the inherent material strength, σ_0 , as follows [34]:

$$L = \frac{1}{\pi} \left(\frac{K_{\text{Ic}}}{\sigma_0} \right)^2 \quad (5)$$

The effective stress, σ_{eff} , required to perform the static assessment according to Eq. (4) has to be calculated by directly post-processing the linear-elastic stress field in the vicinity of the stress concentrator being designed. Effective stress σ_{eff} can be determined according to the Point Method (PM), the Line Method (LM), and the Area Method (AM) as follows [34, 40, 41]:

$$\sigma_{\text{eff}} = \sigma_y \left(\theta = 0, r = \frac{L}{2} \right) \quad (\text{PM}) \quad (6)$$

$$\sigma_{\text{eff}} = \frac{1}{2L} \int_0^{2L} \sigma_y(\theta = 0, r) dr \quad (\text{LM}) \quad (7)$$

$$\sigma_{\text{eff}} = \frac{4}{\pi L^2} \int_0^{\pi/2} \int_0^L \sigma_1(\theta, r) r dr d\theta \quad (\text{AM}) \quad (8)$$

The adopted symbols as well as the meaning of the effective stress calculated through definitions (6) to (8) are explained in Figures 3a to 3d, with σ_y being the stress parallel to axis y and σ_1 the maximum principal stress.

According to Eqs (6) to (8), the determination of the effective stress is based on the use of a suitable critical distance, where, given the experimental value of the plane strain fracture toughness, L can be determined directly via Eq. (5) solely for those brittle materials for which σ_o is invariably equal to σ_{UTS} . In contrast, when σ_o is different from σ_{UTS} (as for ductile materials), the required characteristic length has to be determined by post-processing the results generated by testing specimens containing notches of different sharpness [34, 38]. This procedure is schematically shown in Figure 3e. In particular, according to the PM's *modus operandi*, the coordinates of the point at which the two linear-elastic stress-distance curves, plotted in the incipient failure condition, intersect each other allow L and σ_o to be estimated directly. To conclude, it is worth recalling here that this experimental procedure based on notches of different sharpness is seen to be very accurate also in estimating K_{Ic} [42]. In more detail, as soon as both L and σ_o determined according to the procedure schematically depicted in Figure 3e are known, the

plane strain fracture toughness for the specific material being investigated can directly be estimated through Eq. (5), with K_{Ic} being now the unknown variable in the problem.

4. Extending the use of the TCD to situations involving dynamic loading

As discussed above, examination of the state of the art suggests that the strength and fracture toughness of concrete subjected to dynamic loading are different from the corresponding values determined under quasi-static loading. If these experimental findings are reinterpreted according to the TCD's *modus operandi*, one may argue that, since, as per Eqs (2) and (3), both the strength and the fracture toughness of concrete follow a power law as the rate of the applied loading increases, both inherent strength σ_0 and length scale parameter L should vary the same way as $\dot{\epsilon}$ increases [43]. In particular, by using \dot{Z} to denote either the loading rate, the strain rate, the displacement rate, or the stress intensity factor (SIF) rate, according to Eqs (2) and (3) the effect of the dynamic loading on both the failure stress and the fracture toughness can be expressed as follows [43]:

$$\sigma_f(\dot{Z}) = f_{\sigma_f}(\dot{Z}) = \alpha_{\sigma_f} \cdot \dot{Z}^{\beta_{\sigma_f}} \quad (9)$$

$$K_{Id}(\dot{Z}) = f_{K_{Id}}(\dot{Z}) = \alpha_{K_{Id}} \cdot \dot{Z}^{\beta_{K_{Id}}} \quad (10)$$

where $f_{\sigma_f}(\dot{Z})$ and $f_{K_{Id}}(\dot{Z})$ are functions which can be either determined by running appropriate experiments or derived theoretically.

Recalling that, under static loading, σ_0 is seen to be equal to σ_{UTS} for brittle materials, it can be hypothesised that, similar to the dynamic failure stress, Eq. (9), also the inherent material strength varies with \dot{Z} according to a power law, i.e.:

$$\sigma_0(\dot{Z}) = f_{\sigma_0}(\dot{Z}) = \alpha_{\sigma_0} \cdot \dot{Z}^{\beta_{\sigma_0}} \quad (11)$$

where, again, function $f_{\sigma_0}(\dot{Z})$ can be either determined experimentally or derived theoretically. According to the hypotheses formed above, in the most general case, length scale parameter L as well is expected to change as dynamic variable \dot{Z} varies, in fact [43]:

$$L(\dot{Z}) = \frac{1}{\pi} \left[\frac{K_{Ic}(\dot{Z})}{\sigma_0(\dot{Z})} \right]^2 = \alpha_L \cdot \dot{Z}^{\beta_L} \quad (12)$$

Having defined the laws needed to describe the way both the inherent material strength and the critical distance value vary under dynamic loading, according to the TCD's philosophy the dynamic effective stress, $\sigma_{\text{eff}}(\dot{Z})$, can then be defined as follows (for an explanation of these definition the reader is referred to the static case as described in Figure 3):

$$\sigma_{\text{eff}}(\dot{Z}) = \sigma_y \left(\theta = 0, r = \frac{L(\dot{Z})}{2} \right) \quad (\text{PM}) \quad (13)$$

$$\sigma_{\text{eff}}(\dot{Z}) = \frac{1}{2L(\dot{Z})} \int_0^{2L(\dot{Z})} \sigma_y(\theta = 0, r) \, dr \quad (\text{LM}) \quad (14)$$

$$\sigma_{\text{eff}}(\dot{Z}) = \frac{4}{\pi L(\dot{Z})^2} \int_0^{\pi/2} \int_0^{L(\dot{Z})} \sigma_1(\theta, r) \, r \, dr \, d\theta \quad (\text{AM}) \quad (15)$$

where the stress analysis is still carried out by using a linear-elastic constitutive law. In other words, as postulated by the TCD [34], the hypothesis is formed that the behaviour of notched concrete subjected to dynamic loading can be modelled directly via $\sigma_0(\dot{Z})$ and $L(\dot{Z})$ without taking into account the actual non-linear stress vs. strain dynamic response of the material being assessed.

Eqs (9) to (12) make it evident that the proposed reformulation of the TCD is based on the use of simple power laws. The main advantage of using this type of mathematical functions is that power laws are not only simple to calibrate, but also straightforward to employ to estimate the strength

of notched plain concrete. Unfortunately, this simplicity results in the fact that the required constants are measured in units that are obviously unconventional. Having considered this important aspect very carefully, we decided to keep using power laws in any case not only because they have proven to be very accurate in estimating the dynamic strength of other materials [43], but also because the ultimate goal of the present paper is promoting a simple design method that is suitable for performing rapid calculations in situations of practical interest.

Turning to the design issue, according to the assumptions briefly discussed above, notched concrete components experiencing in-service dynamic loading are then supposed not to fail as long as the following conditions is assured:

$$\sigma_{\text{eff}}(\dot{Z}) < \sigma_0(\dot{Z}) \quad (16)$$

Owing to the complexity of the reasoning on which the design method being proposed is based, a set of suitable experimental results is obviously needed to check the validity of the formed hypotheses. This will be done in the next sections.

5. Experimental details

To check the accuracy of the novel reformulation of the TCD presented in the previous section, a series of bending tests involving un-notched and notched specimens of plain concrete were run in the Structural Engineering Laboratory of the University of Sheffield, UK.

This experimental investigation involved 100 mm x 100 mm square section beams weakened by notches of different sharpness and loaded in four-point bending. The length of the notched samples was equal to 500mm and the nominal notch depth to 50mm. These beams contained U-notches having root radius, r_n , equal to 25 mm (resulting in a stress concentration factor, K_t , equal to 1.47), 12.5 mm ($K_t=1.84$), and 1.3 mm ($K_t=4.99$). For the sake of clarity, the geometries of the tested notched specimens are shown in Figure 4. The strength of the un-notched material was

determined instead by testing under three-point bending rectangular section specimens having width equal to 100mm and thickness to 50mm (i.e., having the same net cross-sectional area as the notched specimens).

The concrete mix used to cast the specimens was as follows [44]: Portland cement (strength class equal to 30 N/mm²), natural round gravel (10 mm grading), and grade M sand. The water-to-cement ratio was set equal to 0.45. A high workability was achieved to ensure that coarse aggregates were distributed as uniformly as possible around the notches. The specimens were removed from the moulds 24 hours after casting and subsequently cured in a moist room for 28 days at 23°C. The notched specimens with notch root radius equal to 25 mm and 12.5 mm were manufactured by casting the required geometrical features into the bulk material through plastic inserts directly attached to the bottom of the moulds. The sharp notches instead were machined by using a circular saw.

To generate the results used to check the accuracy of the TCD as reformulated in the previous section, the specimens were arranged in a simply supported configuration, where the upper supports were able to move vertically by means of a hydraulic actuator. The notched samples were tested under four-point bending, whereas the un-notched specimens under three-point bending. The actuator was load-controlled and was operated via two feed/relief valves. These valves controlled both the loading rate and the maximum applied load. The peak load was recorded during testing and a LVDT was used to monitor the vertical displacement of the supports. Displacement rates were quantified by directly post-processing the signals measured using the LVDT. In order to determine $\dot{\Delta}$ accurately, the initial shift due to the vertical rigid motion of the specimens was removed from the gathered data, with this being done by directly monitoring the change in the slope of the recorded displacement vs. time curves.

The un-notched and notched beams were tested by exploring displacement rates, $\dot{\Delta}$, in the range $3 \cdot 10^{-4}$ -4.4 mm/s. The experimental results being generated are summarised in the charts of Figures 5a to 5c in terms of failure nominal stress referred to the net area. Further, in the same

diagrams the trend lines obtained by re-analysing the different data sets are also reported, with these trend lines being determined by using the standard least-squares method. As to the reported interpolation power laws, it is interesting to observe that even if they were calculated using continuum mechanics linear-elastic stresses in Figure 5a and nominal net stresses in Figures 5b, 5c and 5d, the calibration constants are characterised by very consistent values in terms of dynamic scaling. This further confirms the validity and reliability of the experimental results that were generated.

To conclude, Figure 6 shows some examples of the cracking behaviour displayed by the notched beams under different displacement rates. In particular, the direct inspection of the fracture surfaces revealed that de-bonding between aggregates and cement paste was the primary failure mechanisms, with this holding true independently of the applied displacement rate.

6. Validation by experimental results

To check the accuracy of the proposed reformulation of the TCD in predicting the strength of the notched samples we tested under both static and dynamic loading, the necessary linear-elastic stress fields in the vicinity of the notches being investigated were determined numerically by using commercial Finite Element (FE) software ANSYS®. The tested concrete was modelled as a homogenous and isotropic material. The FE models were meshed using bi-dimensional elements Plane 183, with the mesh density in the vicinity of the notch tips being increased gradually until convergence occurred. It is important to point out here that the dimensions of the notches in the solved FE models were taken equal to the corresponding average values determined by considering, for any notch geometry, the entire population of the specimens that were tested.

As to the numerical modelling, it is worth observing here that, according to the hypothesis that is usually formed to apply the LEFM concepts to concrete [45], the intrinsic heterogeneous nature of the material was disregarded. Whilst this assumption may result in a certain loss of accuracy, it is the Authors' opinion that this simplifying hypothesis is in any case acceptable because the

TCD is based on the same fundamental assumptions as those used to formalise conventional LEFM [34]. In this context, certainly, an interesting venue worth being explored would be modelling the complex micro/meso/macro-structure of plain concrete by employing specific length scale parameters that are directly related to the size of the dominant source of material heterogeneity [46]. However, since the core aim of the present work is to propose and validate a simple engineering approach suitable for performing rapid calculations, in line with the fundamental hypothesis on which LEFM is based (that applies also to un-reinforced concrete [45]), the required linear-elastic stress fields were determined by simply treating the tested concrete as an homogenous and isotropic material.

Since the tested concrete was characterised by a mechanical behaviour that was predominantly brittle, the hypothesis was formed that inherent strength σ_0 could be taken invariably equal to the un-notched material failure stress [36]. This hypothesis was assumed to hold true independently from the value of the displacement rate being investigated. After making this initial simplifying assumption, owing to the failure strength vs. displacement rate behaviour displayed by the un-notched concrete (see Figure 5a), the σ_0 vs. $\dot{\Delta}$ relationship was expressed by adopting a simple power law - as per Eq. (11). In particular, by employing the standard least-squares method to re-analyse the results plotted in Figure 5a, the following relationship was derived:

$$\sigma_0(\dot{\Delta}) = \sigma_f(\dot{\Delta}) = 6.71 \cdot \dot{\Delta}^{0.0344} \text{ MPa} \quad (17)$$

The critical distance value, L , needed to calculate $\sigma_{eff}(\dot{\Delta})$ according to definitions (13) to (15) was estimated by following the simplified procedure schematically shown in Figure 7. In particular, the results generated by testing both the un-notched and the sharply U-notched specimens were used as calibration information [34, 36, 38], L being determined by making $\dot{\Delta}$ vary in the range of interest. This procedure returned a value for L that was invariably equal to 4.8 mm, i.e.:

$$L(\dot{\Delta}) = 4.8 \text{ mm} \quad (18)$$

In other words, contrary to what we have observed in notched metallic materials subjected to dynamic loading [43], for the specific concrete material being investigated the critical distance was seen not to be affected by the rate of the applied loading. However, it is the authors' opinion that this is a particularly favourable result, so that, in the most general case, L is expected to vary as the loading rate increases (and, in particular, it is expected to increase with the increase of $\dot{\Delta}$). As to the value for L that was estimated according to the procedure discussed above, it is interesting to observe also that this length was seen to be very close to the average inter-aggregate distance that was measured to be equal to about 5 mm. This seems to further confirm that, in the TCD formulation, L is a length scale parameter that is closely related to the characteristics of the dominant source of microstructural heterogeneity [34].

The error diagram of Figure 8 summarises the overall accuracy that was obtained by applying the TCD in the form of the PM, LM, and AM, with the error being calculated using the following standard relationship:

$$Error = \frac{\sigma_{eff}(\dot{\Delta}) - \sigma_0(\dot{\Delta})}{\sigma_0(\dot{\Delta})} [\%] \quad (19)$$

According to the chart of Figure 8, the use of both the PM and AM was seen to result in estimates falling within an error interval of $\pm 20\%$. The LM instead returned predictions that were slightly non-conservative, even if they still fell mainly within the target error band.

In regard to the obtained accuracy, it is worth pointing out here that the proposed reformulation of the TCD was applied by hypothesising that damage always reached its maximum value on those planes parallel to the notch bisector. However, Figure 6 shows that, in some cases, cracks were

seen to initiate away from the notch tip, with the following propagation occurring along directions that were not parallel to the notch bisector. Clearly, this complex cracking behaviour has to be ascribed to the actual local morphology/inhomogeneity of the material in the critical regions of the specimens being tested. Further, it was observed that, due to the effect of the large thickness, even if some cracks initiated at the notch tip, the fact that the initiation point was away from the lateral surfaces resulted in a subsequent growth occurring on planes that were not perfectly aligned to the notch bisector. However, since this complex cracking behaviour has been observed also in other notched materials (such as, for instance, polymers that are classically treated as purely homogenous and isotropic [34]), according to the way the TCD is recommended to be applied in situations of practical interest [34], the generated data were post-processed by simply assuming that damage under both static and dynamic loading was maximised on those planes experiencing the maximum opening loading.

It is possible to conclude by observing that the level of accuracy that was obtained is certainly satisfactory since, in the presence of stress concentration phenomena, it is not possible to distinguish between an error of $\pm 20\%$ and an error of 0% as a consequence of those problems that are usually encountered when performing the testing as well as the numerical analyses [34].

7. Conclusions

In the present paper the linear-elastic TCD was reformulated to make it suitable for assessing static and dynamic strength of notched plain concrete. The accuracy and reliability of the proposed design method was then assessed against a number of experimental results generated by testing, under different displacement rates, plain concrete beams containing notches of different sharpness. The most important conclusions are summarised in what follows.

- The proposed design methodology is suitable for designing notched plain concrete against static and dynamic loading by directly post-processing the linear-elastic stress fields acting on the material in the vicinity of the geometrical features being assessed.

- By adopting simple calibration power laws, the proposed reformulation of the TCD allows reliable static and dynamic assessment to be performed without the need to invoke complex non-linear constitutive laws.
- The TCD used in the form of both the PM and AM was seen to be capable of estimates falling within an error interval of $\pm 20\%$.
- More work needs to be done to extend the use of this design approach based on the TCD to those situations involving static and dynamic multiaxial loading.

References

- [1] B. Hopkinson, A method of measuring the pressure in the detonation of high explosives or by the impact of bullets, Proc. R. Soc. London. Ser. A, Contain. Pap. a Math. Phys. Character. 89 (1914) 411–413.
- [2] R.M. Davies, A critical study of the Hopkinson pressure bar, Philos. Trans. R. Soc. A. 240 (1948) 375–457.
- [3] H. Kolsky, An Investigation of the Mechanical Properties of Materials at very High Rates of Loading, Proc. Phys. Soc. London. B62 (1949) 676–687.
- [4] F.M. Mellinger, D.L. Birkimer, Measurement of Stress and Strain on Cylindrical Test Specimens of Rock and Concrete under Impact Loading, Technical Report No. 4-46, U.S. Army Corps of Engineers, Ohio River Division Laboratories, Cincinnati, USA, 1966.
- [5] L.J. Malvar, C.A. Ross, Review of Strain Rate Effects for Concrete in Tension, ACI Mater. Journals 95 (1998) 735–739.
- [6] T. Ngo, P. Mendis, A. Whittaker, A Rate Dependent Stress-Strain Relationship Model for Normal , High and Ultra-High Strength Concrete, Int. J. Prot. Struct. 4 (2013) 451–466.
- [7] J. Reji, S.P. Shah, Mixed-mode Fracture of Concrete subjected to Impact Loading, J. Struct. Eng. 116 (1990) 585–602.
- [8] D.E. Lambert, C.A. Ross, Strain Rate Effects on Dynamic Fracture and Strength, Int. J. Impact Eng. 24 (2000) 985–998.
- [9] F. Min, Z. Yao, T. Jiang, Experimental and Numerical Study on Tensile Strength of Concrete under Different Strain Rates, Sci. World J. 2014 (2014), Article ID 173531, <http://dx.doi.org/10.1155/2014/173531>.
- [10] A.J. Zielinski, Concrete structures under impact loading Rate effects, Report Stevin Laboratory, Concrete Structures 5-84-14, Delft University of Technology, Faculty Civil Engineering and Geosciences, Institutional Repository, 1984.

- [11] Z.P. Bazant, R. Gettu, Rate Effects and Load Relaxation in Static Fracture of Concrete, *ACI Mater. Journals.* 89 (1992) 456–468.
- [12] P. Rossi, F. Toutlemonde, Effect of loading rate on the tensile behaviour of concrete : description of the physical mechanisms, *Mater. Struct.* 29 (1996) 116–118.
- [13] S.P. Shah, S.E. Swartz, C. Ouyang, *Fracture Mechanics of Concrete*, Wiley Interscience, New York, 1995.
- [14] H. Mihashi, M. Izumi, A stochastic theory for concrete fracture, *Cem. Concr. Res.* 7 (1977) 411–421.
- [15] X. Chen, S. Wu, J. Zhou, Y. Chen, A. Qin, Effect of Testing Method and Strain Rate on Stress-Strain Behavior of Concrete, *J. Mater. Civ. Eng.* 25 (2013) 1752–1761.
- [16] E. Bruhwiler, F.H. Wittmann, Failure of dam concrete subjected to seismic loading conditions, *Eng. Fract. Mech.* 35 (1990) 565–571.
- [17] X.Q. Zhou, H. Hao, Modelling of compressive behaviour of concrete-like materials at high strain rate, *Int. J. Solids Struct.* 45 (2008) 4648–4661.
- [18] F. Ragueneau, F. Gatuingt, Inelastic behavior modelling of concrete in low and high strain rate dynamics, *Comput. Struct.* 81 (2003) 1287–1299.
- [19] D. Zheng, Q. Li, An explanation for rate effect of concrete strength based on fracture toughness including free water viscosity, *Eng. Fract. Mech.* 71 (2004) 2319–2327.
- [20] S. Xiao, H. Li, P.J.M. Monteiro, Influence of strain rates and load histories on the tensile damage behaviour of concrete, *Mag. Concr. Res.* 62 (2010) 887–894.
- [21] L.J. Malvar, J.E. Crawford, Dynamic Increase Factors, Twenty-Eighth DDESB Seminar, Orlando, Florida, August 1998.
- [22] S. Das Adhikary, B. Li, State-of-the-art review on low-velocity impact response of reinforced concrete beams, *Mag. Concrete Res.* 68 (4) (2016) 701-723.
- [23] X. Chen, S. Wu, J. Zhou, Experimental study on dynamic tensile strength of cement mortar using split Hopkinson pressure bar technique, *J. Mater. Civ. Eng.* 26 (6) (2014) doi:10.1061/(ASCE)MT.1943-5533.0000926.
- [24] P. Soroushian, K. Choi, A. Alhamad, Dynamic Constitutive Behavior of Concrete, *ACI J.* (1986) 251–259.
- [25] FIP, CEB-FIP Model Code 1990, Redwood Books, Wiltshire, UK, 1993.
- [26] Li_Qingbin, Zhang_Chuhan, Wang_Guanglun, Dynamic damage constitutive model of concrete in uniaxial tension, *Eng. Fract. Mech.* 53 (1996) 449–455.
- [27] J.W. Tedesco, C.A. Ross, Strain-Rate Dependent Constitutive Equations for Concrete, *J. Press. Vessel Technol.* 120 (1998) 1053–1067.

- [28] J.W. Tedesco, J.C. Powell, C.A. Ross, M.L. Hughes, A Strain-Rate-Dependent Concrete Material Model For ADINA, *Comput. Struct.* 64 (1997) 1053–1067.
- [29] D.L. Grote, S.W. Park, M. Zhou, Dynamic behavior of concrete at high strain rates and pressures: I. Experimental Characterization, *Int. J. Impact Eng.* 25 (2001) 869–886.
- [30] Q.M. Li, H. Meng, About the Dynamic Strength Enhancement of Concrete-like Materials in a Split Hopkinson Pressure Bar Test, *Int. J. Solids Struct.* 40 (2003) 343–360.
- [31] M. Katayama, M. Itoh, S. Tamura, M. Beppu, T. Ohno, Numerical Analysis Method for the RC and Geological Structures subjected to Extreme Loading by Energetic Materials, *Int. J. Impact Eng.* 34 (2007) 1546–1561.
- [32] X.Q. Zhou, H. Hao, Mesoscale Modelling of Concrete Tensile Failure Mechanism at High Strain Rates, *Comput. Struct.* 86 (2008) 2013–2026.
- [33] S. Midness, N. Banthia, C. Yan, The Fracture Toughness of Concrete under Impact Loading, *Cem. Concr. Res.* 17 (1987) 231–241.
- [34] D. Taylor, *The Theory of Critical Distances: A new perspective in fracture mechanics*, Elsevier, Oxford, UK, 2007.
- [35] H. Askes, L. Susmel, Understanding cracked materials: Is Linear elastic fracture mechanics obsolete?, *Fatigue Fract. Eng. Mater. Struct.* 38 (2015) 154–160.
- [36] L. Susmel, D. Taylor, The Theory of Critical Distances to predict Static Strength of Notched Brittle Components subjected to Mixed-Mode Loading, *Eng. Fract. Mech.* 75 (2008) 534–550.
- [37] L. Susmel, D. Taylor, On the use of the Theory of Critical Distances to predict Static Failures in Ductile Metallic Materials containing different Geometrical Features, *Eng. Fract. Mech.* 75 (2008) 4410–4421.
- [38] L. Susmel, D. Taylor, The Theory of Critical Distances to estimate the static strength of notched samples of Al6082 loaded in combined tension and torsion. Part II: Multiaxial static assessment, *Eng. Fract. Mech.* 77 (2010) 470–478.
- [39] L. Susmel, D. Taylor, The Theory of Critical Distances to estimate the static strength of notched samples of Al6082 loaded in combined tension and torsion. Part I: Material cracking behaviour, *Eng. Fract. Mech.* 77 (2010) 452–469.
- [40] H. Askes, P. Livieri, L. Susmel, D. Taylor, R. Tovo, Intrinsic material length, theory of critical distances and gradient mechanics: Analogies and differences in processing linear-elastic crack tip stress fields, *Fatigue Fract. Eng. Mater. Struct.* 36 (2013) 39–55.
- [41] A.A.H. Ameri, J.B. Davison, L. Susmel, On the use of linear-elastic local stresses to design load-carrying fillet-welded steel joints against static loading, *Eng. Fract. Mech.* 136 (2015) 38–57.
- [42] L. Susmel, D. Taylor, The Theory of Critical Distances as an alternative experimental strategy for the determination of K_{Ic} and ΔK_{th} , *Eng. Fract. Mech.* 77 (2010) 1492–1501.

[43] T. Yin, A. Tyas, O. Plekhov, A. Terekhina, L. Susmel, A novel reformulation of the Theory of Critical Distances to design notched metals against dynamic loading, *Mater. Des.* 69 (2015) 197–212.

[44] R.E. Franklin, H.C. Erntroy, D.C. Teychenne, *Design of Normal Concrete Mixes*, Second, Construction Research Communications Ltd, Watford, 1997.

[45] B. L. Karihaloo *Fracture mechanics and structural concrete*. Longman Scientific & Technical, London, UK, 1995.

[46] C. Bagni, H. Askes, L. Susmel, Gradient elasticity: a transformative stress analysis tool to design notched components against uniaxial/multiaxial high-cycle fatigue. *Fatigue Fract. Engng. Mater. Struct.* 39 8, pp. 1012–1029, 2016.

List of Captions

- Table 1.** Summary of suitable expressions to estimate the strength DIF of plain concrete.
- Figure 1.** Tensile DIF vs. strain rate (after Malvar & Crawford [18]).
- Figure 2.** Dynamic fracture toughness, $K_{I,d}$, vs. strain rate according to Reji & Shah [7] as well as to Lamber & Ross [8].
- Figure 3.** Definition of the local systems of coordinates (a); effective stress, σ_{eff} , calculated according to the Point Method (b), Line Method (c), and Area Method (d); experimental determination of σ_o and L based on results generated by testing specimens containing notches of different sharpness (e).
- Figure 4.** Geometry of the notched specimens tested under four-point bending (dimensions in millimetres).
- Figure 5.** Summary of the generated experimental results.
- Figure 6.** Examples of the cracking behavior displayed by the tested specimens under different values of the displacement rate.
- Figure 7.** Procedure based on the use of the un-notched and sharply notched specimens followed to determine the L vs. $\dot{\Delta}$ relationship.
- Figure 8.** Accuracy of the TCD applied in the form of the PM, LM, and AM in estimating static and dynamic strength of notched concrete.

Tables

Dynamic Increase Factor (DIF)		Ref.
Tension	Compression	
	$1.48 + 0.206 (\log \dot{\epsilon}) + 0.0221 (\log \dot{\epsilon})^2$ $\dot{\epsilon} \geq 10^{-5} s^{-1}$	[24]
$\begin{cases} 1, & \dot{\epsilon} < \dot{\epsilon}_s = 3 \cdot 10^{-6} s^{-1} \\ \left(\frac{\dot{\epsilon}}{\dot{\epsilon}_s}\right)^{1.016\alpha_s}, & \dot{\epsilon}_s < \dot{\epsilon} \leq 30 s^{-1} \\ \gamma_s \left(\frac{\dot{\epsilon}}{\dot{\epsilon}_s}\right)^{0.33}, & \dot{\epsilon} > 30 s^{-1} \end{cases}$ $\log \gamma_s = 7.11\alpha_s - 2.33$ $\alpha_s = \frac{1}{10 + \frac{6\sigma_{cs}}{\sigma_{c0}}}; \sigma_{c0} = 10 \text{ MPa}$	$\begin{cases} 1, & \dot{\epsilon} < \dot{\epsilon}_s = 3 \cdot 10^{-6} s^{-1} \\ \left(\frac{\dot{\epsilon}}{\dot{\epsilon}_s}\right)^{1.026\alpha_s}, & \dot{\epsilon}_s < \dot{\epsilon} \leq 30 s^{-1} \\ \gamma_s \left(\frac{\dot{\epsilon}}{\dot{\epsilon}_s}\right), & \dot{\epsilon} > 30 s^{-1} \end{cases}$ $\log \gamma_s = 6.156\alpha_s - 2$ $\alpha_s = \frac{1}{5 + \frac{9\sigma_{cs}}{\sigma_{c0}}}; \sigma_{c0} = 10 \text{ MPa}$	[25]
$1 + 0.1948 \left(\log \frac{\dot{\epsilon}}{\dot{\epsilon}_s}\right) + 0.03583 \left(\log \frac{\dot{\epsilon}}{\dot{\epsilon}_s}\right)^2$ $\dot{\epsilon}_s = 25 \cdot 10^{-6} s^{-1}$		[26]
	$\begin{cases} 1.058 + 0.00965 \log \dot{\epsilon} \geq 1, \dot{\epsilon} \leq 63 s^{-1} \\ -0.289 + 0.785 (\log \dot{\epsilon}) \leq 2.5, \dot{\epsilon} \geq 63 s^{-1} \end{cases}$	[27]
$\begin{cases} 1, & \dot{\epsilon} < \dot{\epsilon}_s = 10^{-6} s^{-1} \\ \left(\frac{\dot{\epsilon}_Z}{\dot{\epsilon}_s}\right)^\delta, & \dot{\epsilon}_s < \dot{\epsilon} \leq 1 s^{-1} \\ \gamma_s \left(\frac{\dot{\epsilon}_Z}{\dot{\epsilon}_s}\right)^{0.33}, & 1 s^{-1} < \dot{\epsilon} < 160 s^{-1} \end{cases}$ $\log \gamma_s = 6\delta - 2$ $\delta = \frac{1}{1 + \frac{8\sigma_{cs}}{\sigma_{c0}}}; \sigma_{c0} = 10 \text{ MPa}$		[5, 21]
$\begin{cases} 1 + 0.1425 (\log \dot{\epsilon} + 5.8456) \geq 1, \dot{\epsilon} \leq 2.32 s^{-1} \\ 1 + 2.929 (\log \dot{\epsilon} - 0.0635) \leq 6, \dot{\epsilon} \geq 2.32 s^{-1} \end{cases}$		[28]
	$\begin{cases} 1.07 + 0.0235 \log \dot{\epsilon}, \dot{\epsilon} \leq 266 s^{-1} \\ -2.64 + 7.22 (\log \dot{\epsilon}) - 4.4 (\log \dot{\epsilon})^2 + \\ + 0.882 (\log \dot{\epsilon})^3, \dot{\epsilon} \geq 266 s^{-1} \end{cases}$	[29]
	$\begin{cases} 1 + 0.03438 (\log \dot{\epsilon} + 1), \dot{\epsilon} \leq 100 s^{-1} \\ + 8.5303 - 7.1372 (\log \dot{\epsilon}) + \\ + 1.729 (\log \dot{\epsilon})^2, \dot{\epsilon} \geq 100 s^{-1} \end{cases}$	[30]
$1 + 0.1 \log \frac{\dot{\epsilon}}{\dot{\epsilon}_s}$		[31]
$\begin{cases} 1, & \dot{\epsilon} < 10^{-4} s^{-1} \\ 1 + 0.26 (\log \dot{\epsilon} + 4.0769), 10^{-4} < \dot{\epsilon} \leq 1 s^{-1} \\ 1 + 2 (\log \dot{\epsilon} + 0.53), & 1 < \dot{\epsilon} \end{cases}$		[32]
$\begin{cases} 1.12 + 0.0225 \log \dot{\epsilon}, \dot{\epsilon} \leq 10 s^{-1} \\ 1.6 + 1.235 (\log \dot{\epsilon}) + \\ + 0.7325 (\log \dot{\epsilon})^2, 50 \geq \dot{\epsilon} \geq 0.1 s^{-1} \end{cases}$	$\begin{cases} 1.12 + 0.0225 \log \dot{\epsilon}, \dot{\epsilon} \leq 10 s^{-1} \\ 1.2275 - 0.3563 (\log \dot{\epsilon}) + \\ + 0.2713 (\log \dot{\epsilon})^2, 10 \geq \dot{\epsilon} \geq 2.32 s^{-1} \end{cases}$	[17]
$1 + 0.0653 \log \frac{\dot{\epsilon}}{\dot{\epsilon}_s}, \dot{\epsilon}_s = 10^{-5} \leq \dot{\epsilon} \leq 10^{-1} s^{-1}$		[20]

Table 1. Summary of suitable expressions to estimate the strength DIF of plain concrete.

Figures

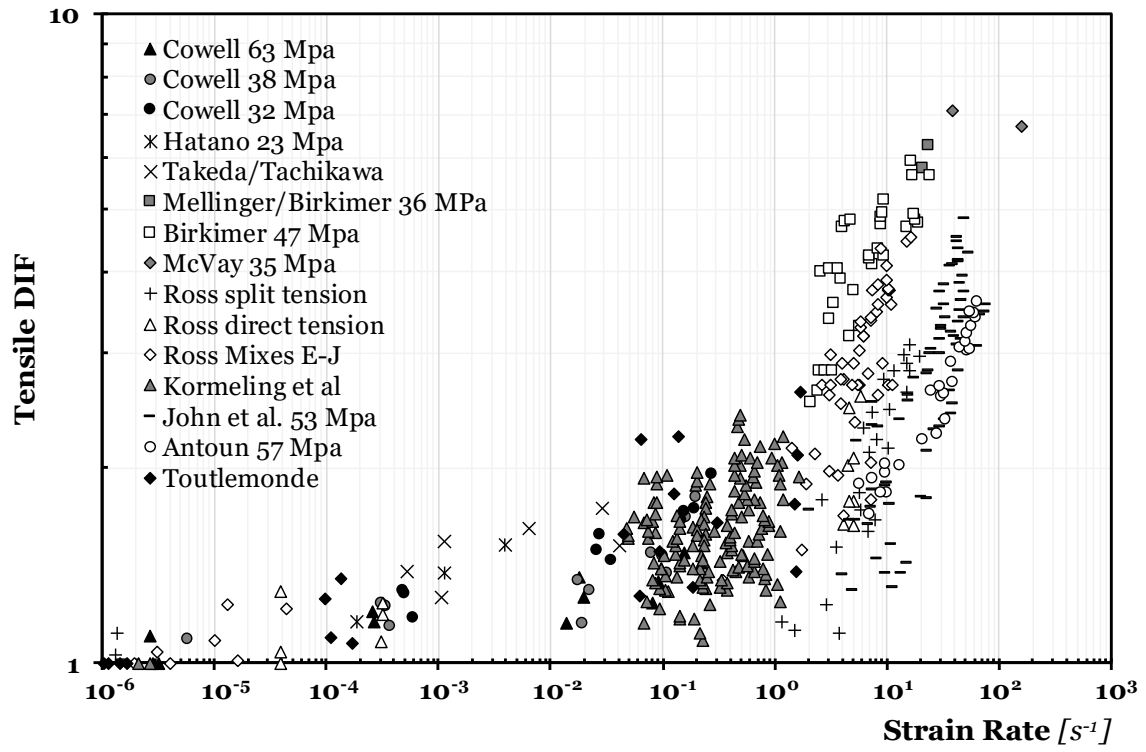


Figure 1. Tensile DIF vs. strain rate (after Malvar & Crawford [21]).

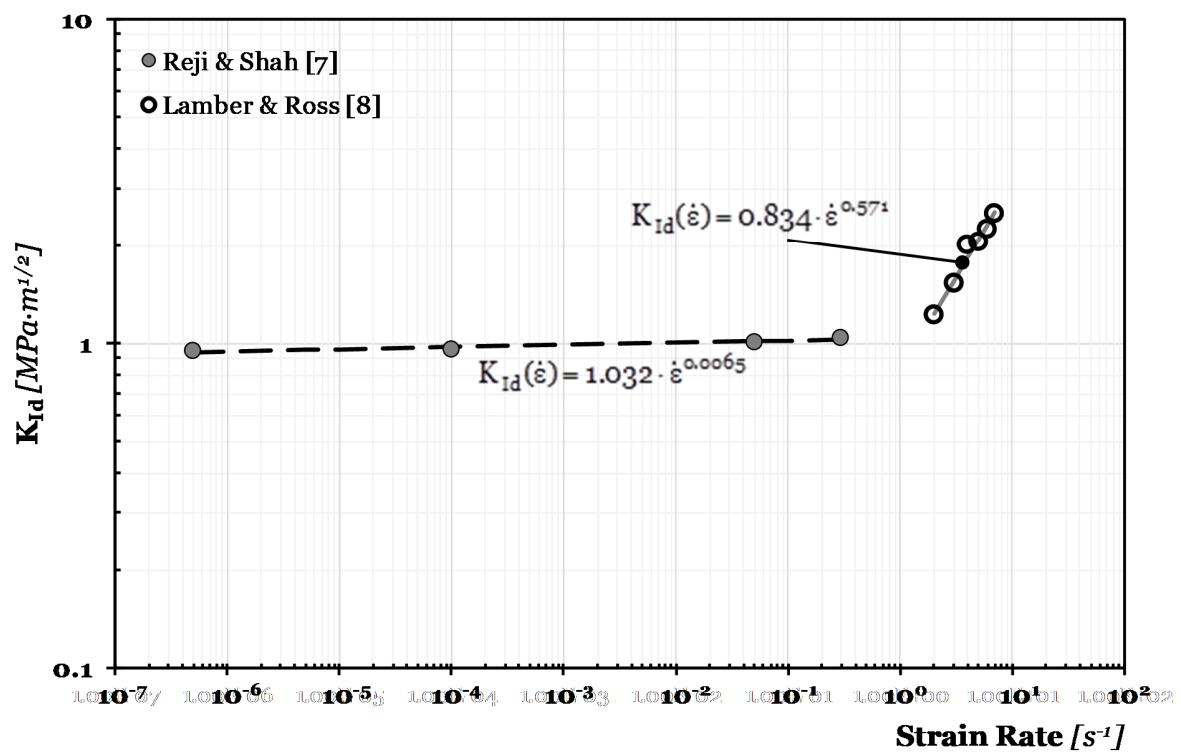


Figure 2. Dynamic fracture toughness, K_{Id} , vs. strain rate according to Reji & Shah [7] as well as to Lamber & Ross [8].

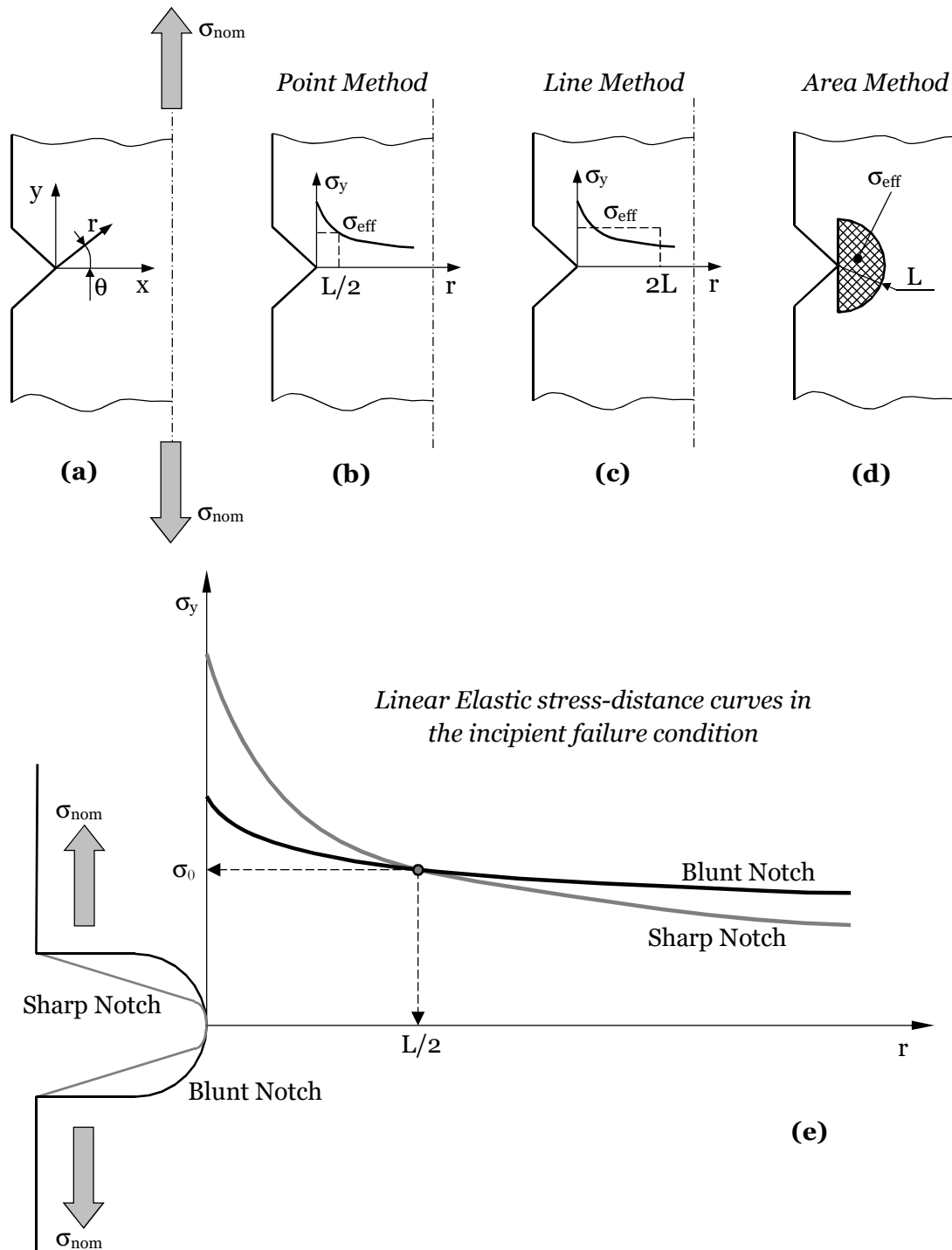


Figure 3. Definition of the local systems of coordinates (a); effective stress, σ_{eff} , calculated according to the Point Method (b), Line Method (c), and Area Method (d); experimental determination of σ_0 and L based on results generated by testing specimens containing notches of different sharpness (e).

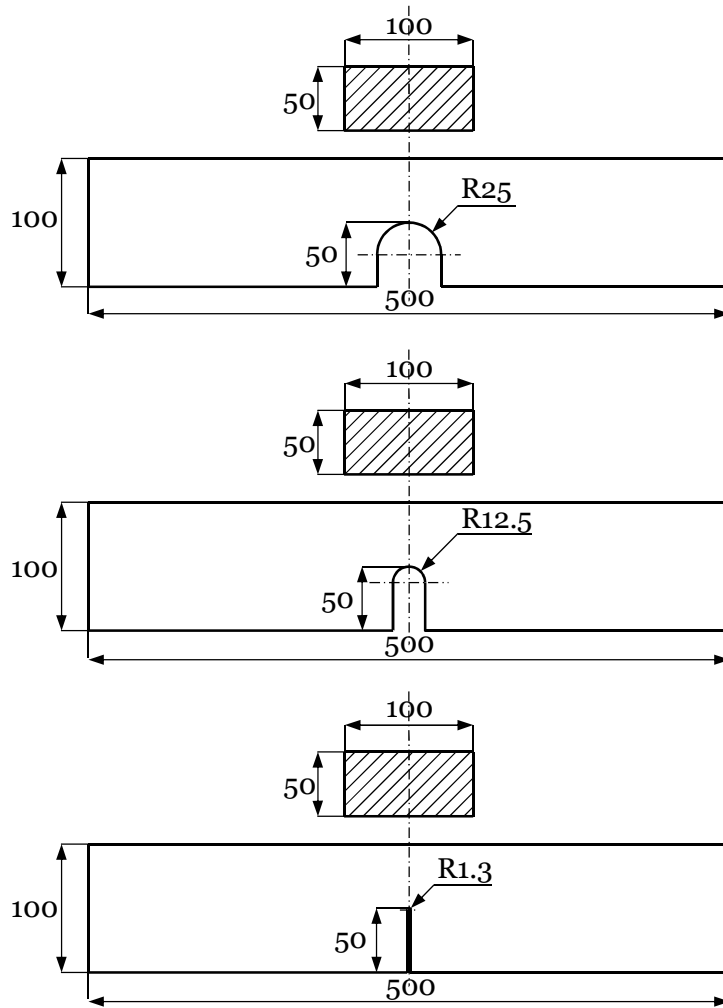


Figure 4. Geometry of the notched specimens tested under four-point bending (dimensions in millimetres).

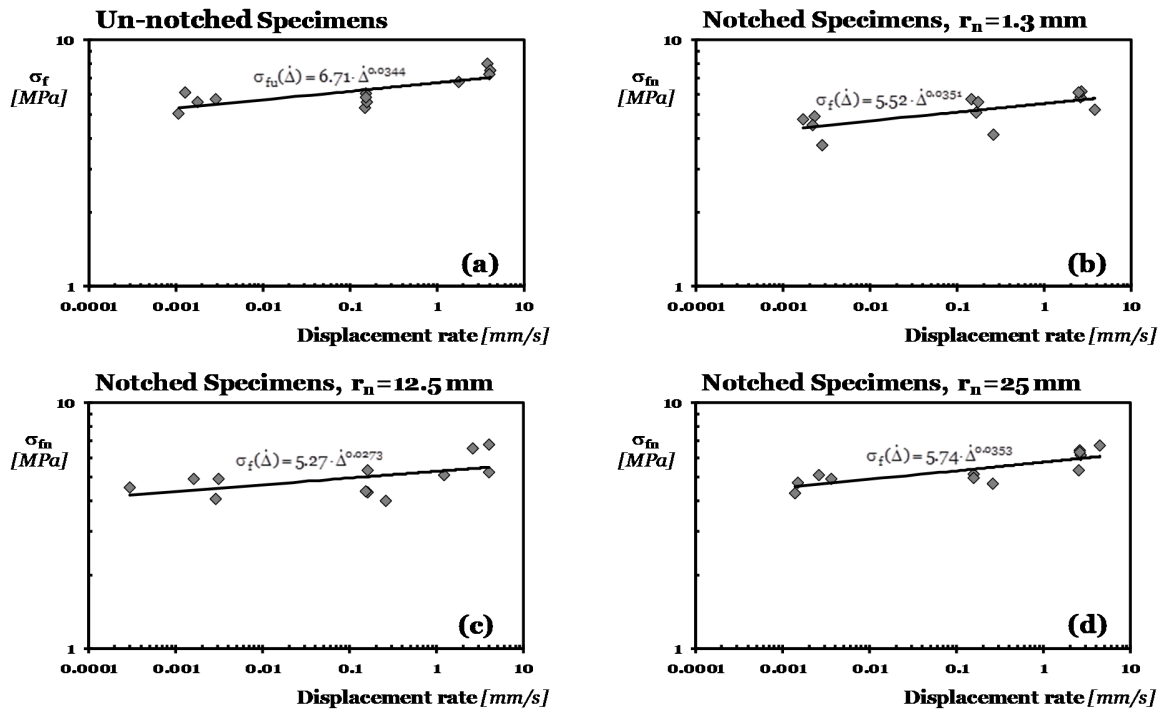


Figure 5. Summary of the generated experimental results.

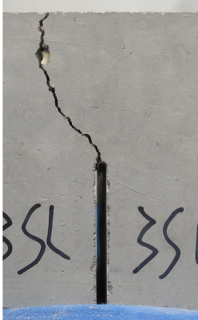
$r_n=25 \text{ mm}$ $K_t=1.47$	 $\dot{\Delta}=0.0014 \text{ mm/s}$	 $\dot{\Delta}=0.26 \text{ mm/s}$	 $\dot{\Delta}=4.44 \text{ mm/s}$
$r_n=12.5 \text{ mm}$ $K_t=1.84$	 $\dot{\Delta}=0.0003 \text{ mm/s}$	 $\dot{\Delta}=0.16 \text{ mm/s}$	 $\dot{\Delta}=4.02 \text{ mm/s}$
$r_n=1.3 \text{ mm}$ $K_t=4.99$	 $\dot{\Delta}=0.0022 \text{ mm/s}$	 $\dot{\Delta}=0.26 \text{ mm/s}$	 $\dot{\Delta}=3.80 \text{ mm/s}$

Figure 6. Examples of the cracking behavior displayed by the tested specimens under different values of the displacement rate.

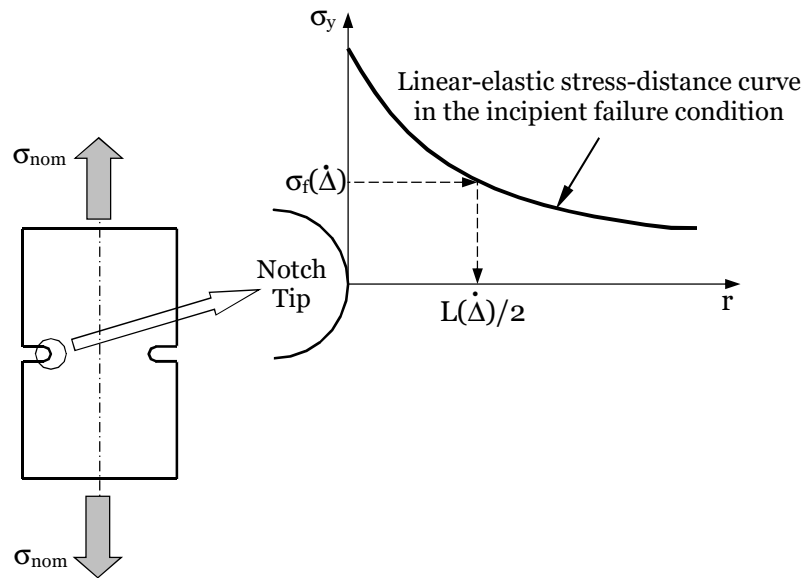


Figure 7. Procedure based on the use of the un-notched and sharply notched specimens followed to determine the L vs. $\dot{\Delta}$ relationship.

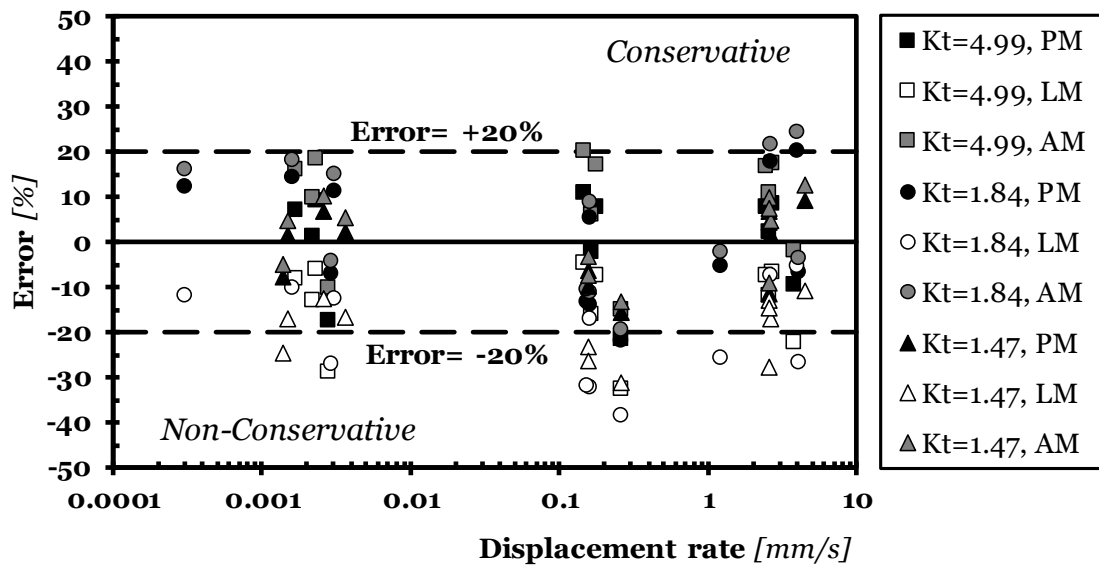


Figure 8. Accuracy of the TCD applied in the form of the PM, LM, and AM in estimating static and dynamic strength of notched concrete.